Hambright, P. H., & Fleischer, E. B. (1970) *Inorg. Chem. 9*, 1757-1761.
Hambright, P. H., Gore, T., & Burton, M. (1976) *Inorg. Chem. 15*, 2314-2315.
Kalyanasundaram, K. (1984) *Inorg. Chem. 23*, 2453-2459.
Kelly, J. M., Murphy, M. J., McConnell, D. J., & OhUigin, C. (1985) *Nucleic Acids Res. 13*, 167-184.
Le Pecq, J. B., & Paoletti, C. (1967) *J. Mol. Biol. 27*, 87-106.
Little, R. G., Anton, J. A., Loach, P. A., & Ibers, J. A. (1975) *J. Heterocycl. Chem. 12*, 343-349.
Marzilli, L. G., Banville, D. L., Zon, G., & Wilson, W. D. (1986) *J. Am. Chem. Soc. 108*, 4188-4192.
Pasternack, R. F., Huber, P. R., Boyd, P., Engasser, L., Francesconi, L., Gibbs, E., Fasella, P., Cerio Venturo, G., & Hinds, L. deC. (1972) *J. Am. Chem. Soc. 94*, 4511-4517.
Pasternack, R. F., Cobb, M. A., & Sutin, N. (1975) *Inorg. Chem. 14*, 866-873.
Pasternack, R. F., Lee, H., Malek, P., & Spencer, C. (1977) *J. Inorg. Nucl. Chem. 39*, 1865-1870.
Pasternack, R. F., Gibbs, E. J., & Villafranca, J. J. (1983a) *Biochemistry 22*, 2406-2414.
Pasternack, R. F., Gibbs, E. J., & Villafranca, J. J. (1983b) *Biochemistry 22*, 5409-5417.
Pasternack, R. F., Antebi, A., Ehrlich, B., Sidney, D., Gibbs, E. J. Bassner, S. L., & DePoy, L. M. (1984) *J. Mol. Catal. 23*, 235-242.
Pasternack, R. F., Gibbs, E. J., Gaudemer, A., Antebi, A., Bassner, S., DePoy, L., Turner, D. H., Willilams, A., Laplace, F., Lansard, M. H., Merienne, C., & Perrée-Fauvet, M. (1985) *J. Am. Chem. Soc. 107*, 8179-8186.
Pasternack, R. F., Garrity, P., Ehrlich, B., Davis, C. B., Gibbs, E. J., Orloff, G., Giartosio, A., & Turano, C. (1986) *Nucleic Acids Res. 14*, 5919-5931.
Reinhardt, C. G., Roques, B. P., & Le Pecq, J. B. (1982) *Biochem. Biophys. Res. Commun. 104*, 1376-1385.
Sari, M. A., Battioni, J. P., Mansuy, D., & Le Pecq, J. B. (1986) *Biochem. Biophys. Res. Commun. 141*, 643-649.
Sari, M. A., Battioni, J. P., Dupré, D., Mansuy, D., & Le Pecq, J. B. (1988) *Biochem. Pharmacol. 37*, 1861-1862.
Saucier, J. M., Festy, B., & Le Pecq, J. B. (1971) *Biochimie 53*, 973-980.
Shamim, A., Hambright, P., & Williams, F. X. (1979) *Inorg. Nucl. Chem. Lett. 15*, 243-246.
Shamim, A., Worthington, P., & Hambright, P. (1981) *J. Chem. Soc. Pak. 3*, 1-3.
Strickland, J. A., Banville, D. L., Wilson, W. D., & Marzilli, L. G. (1987) *Inorg. Chem. 26*, 3398-3406.
Strickland, J. A., Marzilli, L. G., Gay, K. M., & Wilson, W. D. (1988) *Biochemistry 27*, 8870-8878.
Strickland, J. A., Marzilli, L. G., & Wilson, W. D. (1989) *Biopolymers* (in press).
Verlhac, J. P. (1984) Thèse de 3ème cycle, Orsay, France.
Ward, B., Skorobogaty, A., & Dabrowiak, J. C. (1986) *Biochemistry 25*, 7827-7833.

# Solution Conformation of an RNA Hairpin Loop†

Joseph D. Puglisi,‡ Jacqueline R. Wyatt, and Ignacio Tinoco, Jr.*
*Department of Chemistry and Laboratory of Chemical Biodynamics, University of California, Berkeley, California 94720*
*Received October 17, 1989; Revised Manuscript Received January 2, 1990*

ABSTRACT: The hairpin conformation adopted by the RNA sequence $^{5'}$**GCGAUUUCUGACCGCC**$^{3'}$ has been studied by one- and two-dimensional NMR spectroscopy. Exchangeable imino spectra in 60 mM $Na^+$ indicate that the hairpin has a stem of six base pairs (indicated by boldface type) and a loop of three nucleotides. NOESY spectra of nonexchangeable protons confirm the formation of the stem region. The duplex has an A-conformation and contains an A·C apposition; a G·U base pair closes the loop region. The stem nucleotides have C3′-endo sugar conformations, as expected of an A-form duplex, whereas the three loop nucleotides adopt C2′-endo sugar puckers. Stacking within the loop, $C_8$ upon the sugar of $U_7$, stabilizes the structure. The pH dependence of both the exchangeable and nonexchangeable NMR spectra is consistent with the formation of an $A^+$·C base pair, protonated at the N1 position of adenine. The stability of the hairpin was probed by using absorbance melting curves. The hairpin structure with the $A^+$·C base pair is about +2 kcal/mol less stable in free energy at 37 °C than the hairpin formed with an A·U pair replacing the $A^+$·C pair.

Hairpins are common elements of RNA secondary structure. These stem–loop structures are often the building blocks for the three-dimensional folded architecture of RNA. The well-characterized secondary structure of the 16S rRNA from *Escherichia coli* (1542 nucleotides) contains 31 hairpin loop structures (Noller, 1984). The much simpler cloverleaf secondary structure of tRNA contains three hairpin loops. The crystal structures of tRNAs show that hairpin loops are not inert structural elements but can be actively involved in the tertiary structure; the interactions between the D and T loop regions are important to the three-dimensional L-shaped folding of $tRNA^{Phe}$. It has become increasingly clear that stem–loop structures are important sites for specific RNA–protein interactions. The bacteriophage R17 coat protein represses translation of the R17 replicase gene by specific binding to a hairpin that contains the initiation codon (Romaniuk et al., 1987). Both sequence and stem–loop structure determine specific binding interactions (Wu & Uhlenbeck,

† This work was supported in part by the National Institutes of Health under Grant GM 10840 and by the Department of Energy, Office of Energy Research, Office of Health and Environmental Research, under Grant DE-FG03-86ER60406.
* To whom correspondence should be addressed at the Department of Chemistry.
‡ Present address: Institut de Biologie Moleculaire et Cellulaire du CNRS, 15, rue René Descartes, 67084 Strasbourg, France.

0006-2960/90/0429-4215$02.50/0 

1987). In contrast to DNA, protein recognition of a specific sequence in RNA often requires a single-stranded conformation. As in the R17 mRNA, sequestering a sequence within a double-stranded region can inhibit the processes requiring that sequence (ribosome binding). Similar regulatory hairpins have been proposed in other mRNAs (Müllner & Kühn, 1988). Putative hairpin structures are involved in trans activation of the *tat* gene in the HIV virus (Feng & Holland, 1988; Dingwall et al., 1989); the trans activation requires that a sequence CUGGG be within a loop region. Hairpins may thus be crucial for the presentation of specific sequences as single strands. Equilibria among various RNA conformations could play a role in regulating these processes (Wyatt et al., 1990).

Little is known concerning the structure and stability of RNA hairpin loops in solution. Only the anticodon loop of $tRNA^{Phe}$ has been studied both in crystal and in solution (Holbrook et al., 1978; Clore et al., 1984). The relatively large loops in tRNA show considerable stacking, which led Haasnoot and Hilbers to propose that loop sizes of about seven were conformationally most stable in RNA (Haasnoot et al., 1986). Similar conclusions had been reached from thermodynamic data on hairpins with only cytosines in the loops (Gralla & Crothers, 1973; Uhlenbeck et al., 1973). Although tRNA sequences often contain hairpins with loops of seven or eight nucleotides (Rich & RajBhandary, 1976), the 16S rRNA secondary structure mostly contains hairpins with smaller loops of three to six nucleotides (Noller, 1984). Recent thermodynamic studies of hairpin loops containing adenines, uracils, or cytosines shows that loops with four to six nucleotides are most stable in RNA (Groebe & Uhlenbeck, 1988). Loop stabilities also vary with sequence (Tuerk et al., 1988). These loop size and sequence variations should be reflected in structural variations: differences in base stacking and hydrogen bonding within a loop. The presence of stacked nucleotides may account for the stability of the anticodon loops in tRNA. Also, two nucleotides in a loop may interact (for example, $T_{54}$ and $^{m1}A_{58}$ form a Hoogsteen pair in the T loop of $tRNA^{Phe}$).

The formation of non-Watson–Crick base pairs can stabilize any RNA loop sequence. In secondary structures, loop regions are usually written as open and non-base-paired; this method of presentation may be misleading. A large loop with little potential to form Watson–Crick pairs may be closed through formation of nonstandard pairs (Varani et al., 1989). The most commonly considered mispair in RNA is the G·U pairing. Thermodynamic investigations have confirmed the stability of this base pair within an A-form duplex: a G·U pair is approximately as stable as an A·U base pair (Sugimoto et al., 1986). Although mispairs are common within predicted secondary structures, virtually nothing is known about the stability of mispairs other than G·U in RNA duplexes. Crystal structures of DNA have shown that G·T, A·C, and A·G pairings can all be incorporated into a B-DNA duplex (Kennard, 1985; Hunter et al., 1986).

We have investigated by NMR methods the hairpin structure formed by the sequence shown in Figure 1. We were surprised to find that the stem region of the hairpin contains both A·C and G·U pairings (Figure 1b). Conformations of the nucleotides in the loop and of the mispaired bases in the stem of this unique hairpin were determined.

## Materials and Methods

RNA molecules were synthesized, characterized, and purified as described elsewhere (Puglisi et al., 1990). Gel filtration experiments indicated that the molecule was >90% monomeric at strand concentrations as high as 2.5 mM. This

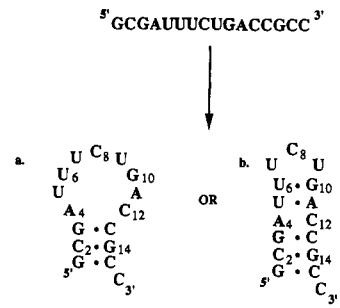


FIGURE 1: (Top) Sequence of the oligonucleotide. (Bottom) Possible folded structures that can be formed. The large loop of nine non-hydrogen-bonded nucleotides (a) can be closed to a loop of only three nucleotides (b) upon formation of extra base pairs.

is an important test, as hairpin sequences can also form double-stranded internal loops. UV absorbance melting curves were obtained and analyzed to give thermodynamic parameters by standard methods (Puglisi & Tinoco, 1989). The melting temperature of the helix-to-coil transition was independent of strand concentration from 0.5 $\mu$M to 1 mM.

Unless noted, all NMR spectra were obtained in 50 mM NaCl, 10 mM sodium phosphate, pH 6.3, and 0.1 mM EDTA on a Nicolet GN-500 spectrometer (500-MHz $^1$H frequency). For pH titrations, the pH was adjusted by using either 0.1 M NaOH or 0.1 M HCl. The pH was monitored with an Orion Research pH meter equipped with an Ingold microelectrode. pH readings in $D_2O$ were uncorrected. $^1$H chemical shifts are referenced to (trimethylsilyl)propionic acid (TSP).

NMR spectra of exchangeable protons were obtained by using a 1–3–3–1 pulse sequence (Hore, 1983). Decoupler spillover was determined by irradiating at variable offsets from a peak. Spillover was estimated to be 100 Hz at the decoupler powers used. Slightly higher power was used for irradiation of the broader G·U imino protons, resulting in >100 Hz spillover. Difference spectra were processed by using 5-Hz line broadening.

$^{31}$P NMR spectra were acquired on a Bruker AM-400 (400-MHz $^1$H frequency) at a frequency of 161.98 MHz using WALTZ broad-band decoupling of protons.

NOESY spectra in $D_2O$ were obtained by using the standard pulse sequence and phase cycling for pure phase spectra (Bodenhausen et al., 1984). Data sets were 4K in $t_2$ with a sweep width of 4464.28 Hz. A total of 500–520 $t_1$ values were collected with 96 scans per $t_1$. A relaxation delay of 2.2–2.5 s was used. Total acquisition time was 24–30 h. NOESY spectra were obtained with a mixing time of 400 ms for assignment of the spectrum and 80 and 120 ms for distance determination. Cross peaks were integrated by using the routine in FTNMR (Infinity Systems). All NOESY spectra were measured at 25 °C. Spectra were processed by using a skewed sine bell function with a 30° phase shift and 0.7 skew.

Distances were approximated from NOE cross-peak volumes at short mixing times. The mixing times of 120 and 80 ms were adequate for measuring intermediate-range distances (>2.5 Å) as checked by the relatively constant H1′–H2′ distances, which were consistent with those expected for a given sugar pucker. Glycosidic torsion angles were estimated from contour plots of interproton distances versus both sugar pucker and glycosidic torsion angle (Wüthrich, 1986; Puglisi, 1989).

Phase-sensitive DQF-COSY spectra were obtained and processed by using the standard pulse sequence (Piantini et al., 1982; Bodenhausen et al., 1984). Data sets were 4K in $t_2$ with a sweep width of 4464.28 Hz. A total of 64 scans were acquired per $t_1$; typical data sets consisted of 500 $t_1$ values. $^{31}$P-broad-band-decoupled DQF-COSY spectra were acquired

with a modification of the standard DQF-COSY pulse sequence such that $^{31}P$ was WALTZ decoupled during $t_2$. Spectral parameters and processing were identical with those for a normal DQF-COSY.

Coupling data were analyzed by a modification of the graphical method of Rinkel and Altona (Rinkel & Altona, 1987; Davis et al., 1989). Coupling constants and sums of coupling constants were estimated from $^{31}P$-decoupled DQF-COSY cross-peak widths. The values of coupling constants and sums of coupling constants ($\sum J$) were related to values of the pseudorotation phase angle ($P$) by a modified Karplus equation (de Leeuw & Altona, 1982; Altona, 1982). Ranges of $P$ are determined that are consistent with all available coupling data (at a maximum pucker amplitude of 40°). An uncertainty in coupling constants of ±1 Hz was assumed.

DQ spectra were acquired and processed as described elsewhere (Puglisi et al., 1990) by using the standard pulse sequence for pure phase spectra (Brauschweiler et al., 1983). Data sets were 4K in $t_2$. A total of 450 $t_1$ values with 64 scans per $t_1$ were acquired for a total experiment time of 20 h.

## Results and Discussion

### *NMR Analysis*

*Assignment of the Exchangeable Proton NMR Spectrum.* The exchangeable proton spectrum of the oligonucleotide at 1 °C is shown in Figure 2a. Gel filtration experiments at NMR concentrations and the RNA concentration independence of the absorbance melting curves showed that the molecule was a monomeric species. We expected that the oligonucleotide would form a hairpin with a stem of three G·C base pairs (Figure 1a). The three sharp resonances between 13.4 and 12.4 ppm are consistent with this expectation. Surprisingly, there are extra resonances present: the peak at 14.53 ppm, due to an A·U base pair, the broad peak centered at 11.3 ppm, most likely due to non-hydrogen-bonded loop imino protons, and the two relatively sharp peaks at 12.07 and 10.75 ppm.

The imino resonances were assigned by using 1-D NOEs. Irradiation of the imino resonance at 12.93 ppm gives NOEs to the peaks at 12.41 and 13.30 ppm. The peak at 12.93 ppm was thus assigned unambiguously to $C_2$·$G_{14}$ pair 2 in the stem region. This assignment was confirmed by separate irradiation of the other two G·C resonances, which each give a single NOE to the resonance at 12.93 ppm. The assignments of the remaining G·C pairs are less definite. Since both resonances only give NOEs to the central G·C imino proton, it was impossible to distinguish the terminal G·C from the internal G·C by NOE data alone. The resonance at 13.30 ppm was assigned as the terminal base pair ($G_1$·$C_{15}$ pair 1) from two other pieces of data. First, the chemical shift of this resonance is the same as in an RNA molecule that forms a pseudoknot structure with the same stem region (Puglisi et al., 1990). Second, the temperature dependence of the imino spectrum (see below) shows that this G·C resonance is the first of the three G·C pair resonances to broaden due to exchange with solvent. Terminal base pairs of a duplex are more accessible to solvent than internal base pairs that close a hairpin loop [see van Knippenberg and Heus (1983)]. The peak at 12.41 ppm is therefore assigned as $G_3$·$C_{13}$ pair 3.

Irradiation of the A·U imino resonance at 14.53 ppm gives a strong NOE to a sharp resonance at 8.07 ppm. In the proposed base pairing, the resonance at 14.53 ppm results from the pair involving $U_5$ and $A_{11}$ (Figure 1). The resonance at 8.07 ppm was assigned to the $A_{11}$(H2) proton. No other NOEs were observed from this imino proton. Irradiation of the resonance at 12.07 ppm gives NOEs to the resonances at 10.75 and 14.53 ppm (Figure 2b). The apparent NOE observed to the resonance at 12.41 ppm is most likely due to decoupler spillover, since the peaks are separated by only 170 Hz; higher decoupler power was used to saturate the two upfield peaks, as required by their greater line width (see Materials and Methods). Irradiation of the resonance at 10.75 ppm gives NOEs to the resonances at 12.07 and 14.53 ppm. Thus, the two upfield resonances (12.07 and 10.75 ppm) have NOEs to each other and to the $U_5$·$A_{11}$ imino resonance.

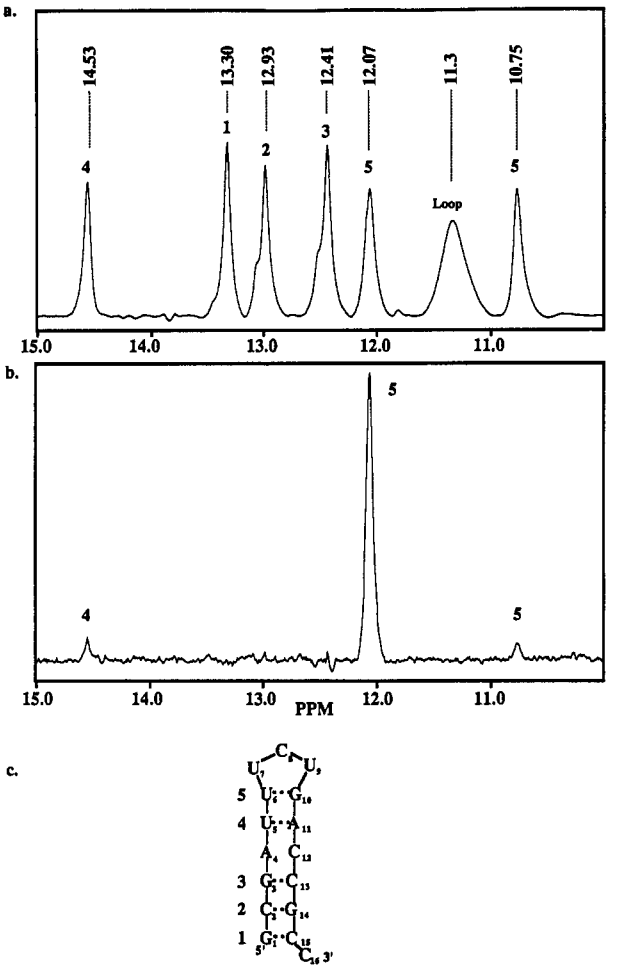


FIGURE 2: (a) NMR spectrum of the exchangeable imino protons in 50 mM NaCl, 10 mM sodium phosphate, pH 6.3, and 0.5 mM EDTA at 5.0 °C; the peaks are numbered according to the assignments made in the text. Chemical shifts in ppm are indicated above each peak. Shoulders on resonances 1 and 2 correspond to the small amount of dimer present. (b) NOE difference spectrum with 600-ms irradiation of the resonance at 12.07 ppm. (c) Schematic folding of the hairpin showing the assignments and numbering scheme of the imino protons.

The data described above suggest that a base pair forms between residues $U_6$ and $G_{10}$. A single G·U base pair gives rise to two imino resonances, since both the G and the U contribute an imino proton to the pair. The chemical shifts of the two upfield peaks at 12.07 and 10.75 ppm are consistent with G·U pair formation. Since the two imino protons are very close (2.2 Å), a G·U pair can generally be identified by the strong NOE between the two resonances. An NOE is observed between these two resonances, but it is not strong. However, the broader line width of these resonances indicates a significant exchange contribution to the spin–lattice relaxation rate, which will weaken observed NOEs. This also explains the lack of an NOE to the G·U resonances upon irradiation of the A·U resonance. NOEs are observed between the G·U

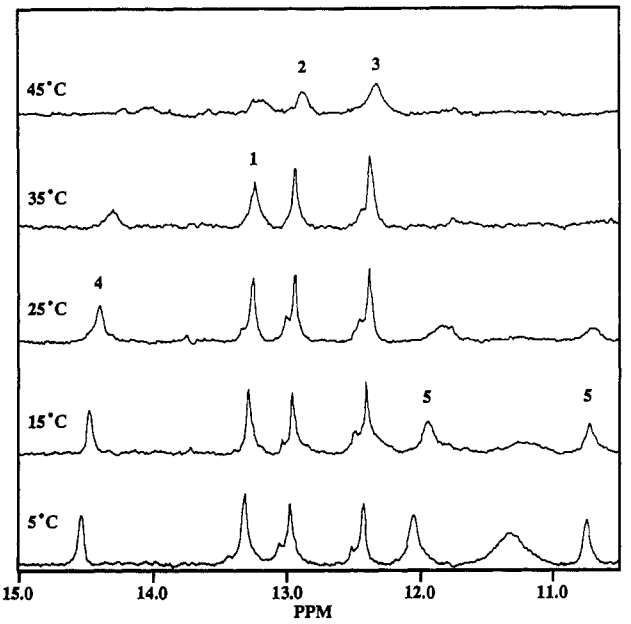


FIGURE 3: Temperature dependence of the exchangeable imino proton NMR spectrum in 50 mM NaCl, 10 mM sodium phosphate, pH 6.3, and 0.5 mM EDTA. Peaks are numbered as in Figure 2c.

resonances and the A·U imino resonance upon irradiation of the G·U peaks. The $U_5$·$A_{11}$ imino proton also does not give any NOE to the stem G·C imino protons, which suggests that the $A_4$·$C_{12}$ apposition is incorporated into the helix. If these bases were squeezed out of the helix, stacking between the $U_5$·$A_{11}$ and the $G_3$·$C_{13}$ pairs should result in an observed NOE between their imino protons. The assignments of the imino protons are summarized in Figure 2c.

*Temperature Dependence of the Exchangeable Spectrum.* Figure 3 shows the NMR spectra of the imino protons as a function of temperature. Except for the broad peak centered at 11.3 ppm, at low temperature (1.5 °C) all resonances are relatively sharp. The broad, unresolved peak corresponds to non-hydrogen-bonded loop imino protons (from $U_7$ and $U_9$); it broadens into base line by 15 °C. The two $U_6$·$G_{10}$ imino resonances broaden first at the same temperature (15 °C), followed by the $U_5$·$A_{11}$ imino resonance at slightly higher temperature. At 25 °C, $G_1$·$C_{15}$ resonance 1 begins to broaden, followed by $C_2$·$G_{14}$ resonance 2 at 35 °C. $G_3$·$C_{13}$ resonance 3 broadens at the highest temperature. The order of imino resonance broadening due to solvent exchange is consistent with the assignment and proposed base-pairing scheme. The U·G and U·A peaks broaden at the lowest temperature, followed by the G·C stem resonances in sequential order from the end of the stem. The imino resonance 3 from $G_3$·$C_{13}$, which is essentially the central base pair, is most protected from solvent exchange. The $U_5$·$A_{11}$ and $U_6$·$G_{10}$ base-pair resonances broaden before that of the terminal base pair, indicating that these pairs are kinetically less stable than the three G·C pairs in the stem.

*Assignment of the Nonexchangeable Proton NMR Spectrum.* The nonexchangeable proton spectrum at 25 °C was assigned by the strategies discussed elsewhere (Puglisi, 1989; Puglisi et al., 1990). The H8/H2/H6–H1′/H5 region of the NOESY spectrum (mixing time = 400 ms) is shown in Figure 4. There are 10 pyrimidine H5–H6 cross peaks; their positions were confirmed by a DQF-COSY experiment. Assignment pathway 1 (Figure 4a) spans six nucleotides with a pattern $^{3'}$Y-Y-R-R-Y-R$^{5'}$ (where Y = pyrimidine and R = purine). This pathway connects the 5′ portion of the oligonucleotide: $^{3'}U_6$-$U_5$-$A_4$-$G_3$-$C_2$-$G_1{}^{5'}$. Assignment pathway 2 (Figure 4b)

Table I: Chemical Shifts (ppm) of the Nonexchangeable Proton NMR Spectrum of the RNA Hairpin[a]

| nucleotide | H8/H6 | H2/H5 | H1′ | H2′ | H3′ | H4′ | H5′/H5″ |
|---|---|---|---|---|---|---|---|
| $G_1$ | 8.22 | | 5.90 | 4.88 | 4.73 | (4.31) | |
| $C_2$ | 7.84 | 5.42 | 5.70 | 4.78 | 4.63 | 4.53 | |
| $G_3$ | 7.65 | | 5.82 | 4.62 | 4.21 | | |
| $A_4$ | 7.99 | 8.29 | 6.16 | 4.63 | 4.56 | 4.21 | |
| $U_5$ | 7.54 | 5.38 | 5.49 | 4.43 | 4.55 | 4.11 | |
| $U_6$ | 7.87 | 5.82 | 5.71 | 3.97 | 4.59 | 4.13 | |
| $U_7$ | 7.95 | 5.92 | 6.06 | 4.50 | 4.30 | | 4.21/4.07 |
| $C_8$ | 7.69 | 5.88 | 5.45 | 4.03 | 4.42 | | |
| $U_9$ | 7.86 | 5.92 | 6.03 | 4.39 | 5.08 | 4.48 | 4.05/3.92 |
| $G_{10}$ | 8.32 | | 6.02 | 5.04 | 4.66 | 4.44 | |
| $A_{11}$ | 8.02 | 8.07 | 6.02 | 4.78 | 4.61 | 4.29 | |
| $C_{12}$ | 7.85 | 5.58 | 5.44 | 4.09 | 4.58 | 4.44 | |
| $C_{13}$ | 7.82 | 5.63 | 5.71 | 4.47 | 4.61 | | |
| $G_{14}$ | 7.65 | | 5.67 | 4.55 | 4.20 | 4.46 | |
| $C_{15}$ | 7.52 | 5.18 | 5.58 | 4.36 | 4.56 | 4.08 | |
| $C_{16}$ | 7.73 | 5.65 | 5.74 | 3.96 | 4.17 | 4.39 | |

[a] Conditions are 50 mM NaCl, 10 mM sodium phosphate, and 0.5 mM EDTA, pH 6.4, 25 °C.

Table II: Summary of *J*-Coupling Data for the Ribose Sugar Protons in the RNA Hairpin

| nucleotide | $J_{1'-2'}$ (Hz) | $\sum J_{2'}$ (Hz) | $\sum J_{3'}$[a] (Hz) | % N |
|---|---|---|---|---|
| $G_1$ | <2 | | | >90 |
| $C_2$ | <2 | | | >90 |
| $G_3$ | <2 | | | >90 |
| $A_4$ | <2 | | 13 | >90 |
| $U_5$ | <2 | | 14 | >90 |
| $U_6$ | <2 | 5.5 | 13 | >90 |
| $U_7$ | 7.7 | 12.9 | 6.7 | <5 |
| $C_8$ | 8.0 | 13.0 | | <5 |
| $U_9$ | 7.4 | 11.5 | 10.7 | 10 |
| $G_{10}$ | 3.0 | 5.6 | 6.5 | 70 |
| $A_{11}$ | <2 | | 13.0 | >90 |
| $C_{12}$ | <2 | | 12.8 | >90 |
| $C_{13}$ | 2.7 | | | 75 |
| $G_{14}$ | <2 | | 13.0 | >90 |
| $C_{15}$ | <2 | | | >90 |
| $C_{16}$ | 2.2 | 5.0 | 13.0 | 85 |

[a] Values for $\sum J_{3'}$ were determined by using $^{31}$P-decoupled DQF-COSY.

spans seven nucleotides with a sequence pattern $^{3'}$Y-Y-R-Y-Y-R-R$^{5'}$. The only nucleotides consistent with this pathway are $^{3'}C_{16}$-$C_{15}$-$G_{14}$-$C_{13}$-$C_{12}$-$A_{11}$-$G_{10}{}^{5'}$. $A_{11}$ and $G_{10}$ have degenerate H1′ resonances. The A(H2) resonances confirm the assignment pathway. The $A_{11}$(H2) resonance (8.07 ppm) was assigned from the 1-D NOEs of the exchangeable protons. This resonance gives NOEs to the $U_6$(H1′) and $C_{12}$(H1′) protons; these are the NOEs expected if the stem region forms an A-form helix. The aromatic proton at 8.04 ppm must be the $A_4$(H2) resonance; it is the only unassigned purine resonance and it has virtually no NOEs to H2′, H4′ or H5′/5″ protons. The $A_4$(H2) proton does have NOEs to the $U_5$ and $C_{13}$(H1′) protons; again, these are the expected NOEs for an A-form helical stem. Three pyrimidine residues are not part of either assignment pathway. These are the three loop nucleotides: $U_7$, $C_8$, and $U_9$.

The assignments were extended by using the H8/H6–H2′/H3′/H4′/H5′/5″ (Figure 5) and H1′–H2′ regions of the NOESY spectrum in conjunction with the DQF-COSY spectrum (Figure 6) (Puglisi, 1989). These assignments are summarized in Table I.

*Analysis of Ribose Conformation Using Spin–Spin Coupling Data.* Spin–spin (*J*) coupling data were obtained from analyses of the coupled and $^{31}$P-decoupled DQF-COSY experiments as described under Materials and Methods. The *J*-coupling data derived from the COSY experiments included $J_{1-2'}$ for all nucleotides; these data are listed in Table II.

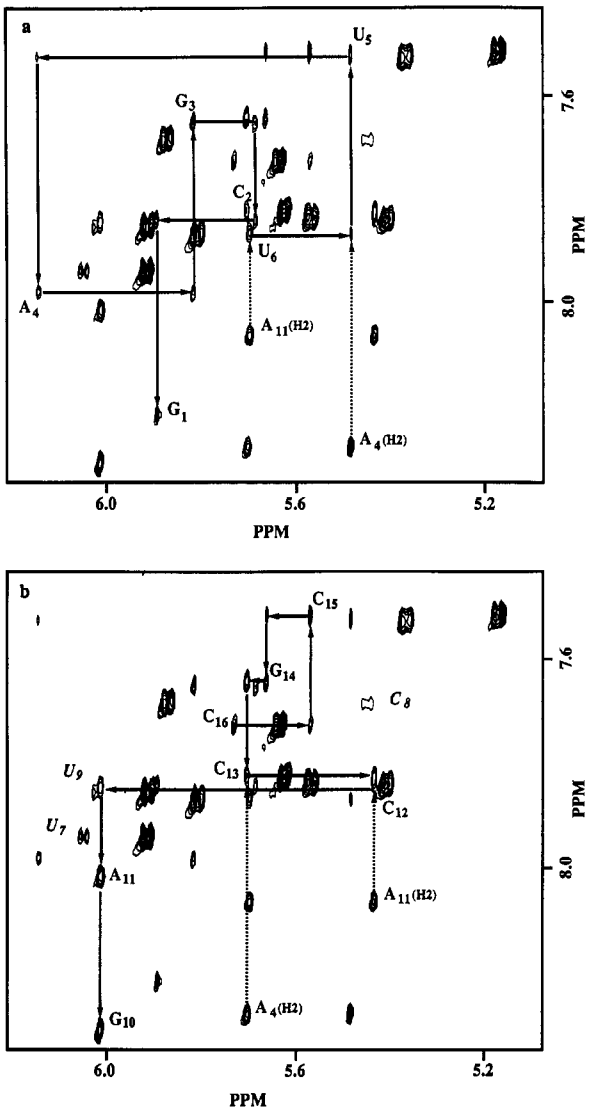


FIGURE 4: Portion of the NOESY spectrum showing NOEs between H8/H6/H2 (7.4–8.4 ppm) and H1′/H5 (5.0–6.2 ppm) protons. The NOESY data were collected in 50 mM NaCl, 10 mM sodium phosphate, pH 6.3, and 0.5 mM EDTA at 25 °C. The mixing time was 400 ms. Labeled NOE cross peaks indicate NOEs from a nucleotide aromatic proton to the H1′ proton on its own sugar. NOEs between A(H2) and H1′ protons are indicated by dotted lines. (a) Aromatic H8/H6–H1′ connectivity pathway 1 (solid line) spans nucleotides $U_6$–$G_1$. (b) NOE connectivity pathway 2, in the same portion of the NOESY spectrum shown in (a), spans nucleotides $C_{16}$–$G_{10}$. NOEs between loop pyrimidine H6 and H1′ protons are italicized.

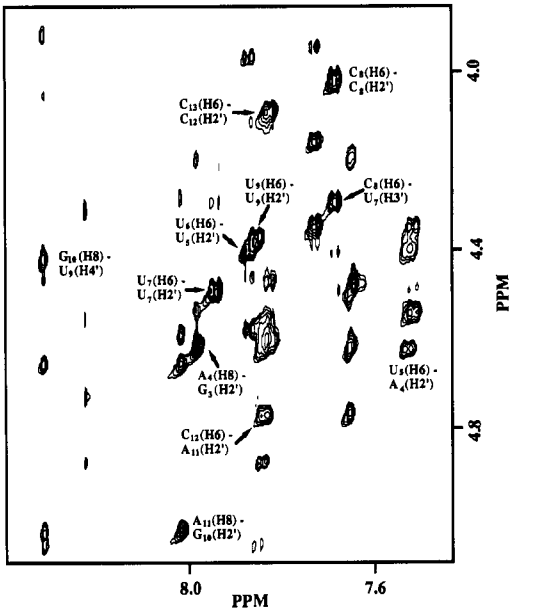


FIGURE 5: Portion of the NOESY spectrum showing NOEs between aromatic H8 and H6 protons (horizontal axis) and sugar H2′, H3′, H4′, and H5′/H5″ protons (vertical axis). The strongest cross peaks result from NOEs between aromatic and sugar H2′ protons. Certain cross peaks important for the structural analysis are labeled.

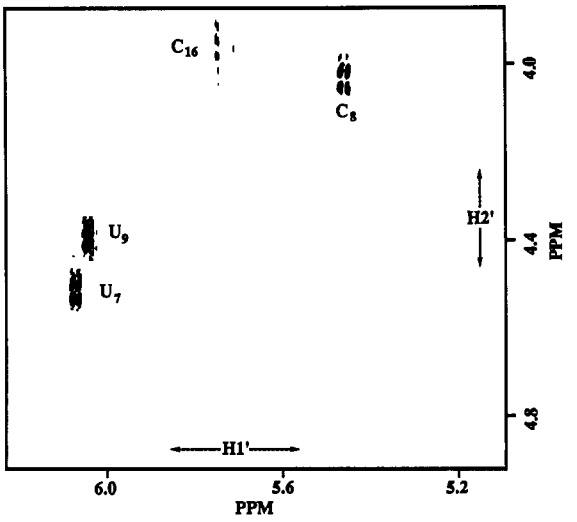


FIGURE 6: Portion of the double-quantum-filtered COSY spectrum showing cross peaks between sugar H1′ and H2′ protons; both positive and negative contours are shown. Only nucleotides with a significant population of S-type (C2′-endo) sugars give observable cross peaks. Nucleotides $U_7$, $C_8$, and $U_9$ give strong cross peaks, whereas $C_{16}$ gives a weaker cross peak. The spectrum was acquired in 50 mM NaCl, 10 mM sodium phosphate, pH 6.3, and 0.1 mM EDTA at 25 °C.

Further coupling data were obtained for certain nucleotides for which cross peaks (H2′–H3′, H3′–H4′) could be assigned in the crowded region near the diagonal in the DQF–COSY spectrum. The total sums of all coupling to either the H2′ ($\sum J_{2'}$) or H3′ ($\sum J_{3'}$) protons are also summarized in Table II.

The $J_{1'-2'}$ value (column 2 of Table II) can be used to approximate whether a certain nucleotide has a relatively pure sugar conformation or an equilibrium mixture of north- ($C_3$-endo) and south- ($C_2$-endo) type sugars in fast exchange. If no H1′–H2′ cross peak was observed in the DQF-COSY, then the value of $J_{1'-2'}$ was assumed to be less than 2 Hz. Splittings that are the same magnitude as the line width lead to cancelation of the antiphase components of a COSY cross peak (Widmer & Wüthrich, 1987; Bax & Lerner, 1988). On the basis of the average line width of the resonances for this oligonucleotide, 2 Hz is the lower limit of observed coupling.

If the sugars are assumed to exist as either north (N) or south (S), then a two-state analysis of the value of $J_{1'-2'}$ can provide the relative populations of each conformer, using the empirical equation of van den Hoogen and Altona (van den Hoogen, 1988):

$$\% \text{ N} = 114.9 - 14.5(J_{1'-2'})$$

The values of $J_{1'-2'}$ were analyzed by this equation to yield the percent north conformation for the nucleotides listed in Table II. Most of the sugars adopt a pure N-type conformation. $G_1$–$U_6$ all have >90% N-type sugars. The stem nucleotides on the 3′ side show slightly more conformational freedom. $G_{10}$ is only 70% N-type, $C_{13}$ is approximately 75% N-type, and the terminal, nonpaired $C_{16}$ also shows conformational freedom (85% N). The loop nucleotides adopt S-type conformations;

Table III: Nucleotide Conformations in the RNA Hairpin

| nucleotide | pseudorotation phase angle ($P$)[a] (deg) | glycosidic torsion angle ($\chi$)[b] (deg) |
|---|---|---|
| $G_1$ | N | anti |
| $C_2$ | N | −170 ± 20 |
| $G_3$ | N | anti |
| $A_4$ | 10 ± 30 | −175 ± 20 |
| $U_5$ | 15 ± 10 | anti |
| $U_6$ | 10 ± 10 | −170 ± 20 |
| $U_7$ | 165 ± 10 | −115 ± 20 |
| $C_8$ | 160 ± 10 | −115 ± 20 |
| $U_9$ | S | −115 ± 20 |
| $G_{10}$ | N/S | anti |
| $A_{11}$ | 5 ± 15 | −180 ± 20 |
| $C_{12}$ | 0 ± 20 | anti |
| $C_{13}$ | N/S | anti |
| $G_{14}$ | 5 ± 15 | −175 ± 20 |
| $C_{15}$ | N | −170 ± 20 |
| $C_{16}$ | N/S | anti |

[a] Pseudorotation phase angles ($P$) were determined as described in the text; where no coupling information other than $J_{1'-2'}$ is available, sugar pucker is listed as either N (C3′-endo) or S ($C_{2'}$-endo). [b] Glycosidic torsion angles were calculated from intranucleotide aromatic–sugar distances listed in Table IV as described. Where no H8/H6–H2′ or H8/H6–H3′ distances are available, $\chi$ is listed as anti.

$U_7$ and $C_8$ have fairly pure S-type conformations, whereas $U_9$ has a small population (10%) of N-type conformer.

A more precise value of the pseudorotation phase angle ($P$) can be estimated by the graphical method described by Rinkel and Altona (1987) and used by Davis et al. (1989). The range of $P$ values consistent with each value of a coupling constant of $J \pm 1$ Hz is determined. Only a small range of $P$ values are consistent with the three sets of data presented for $U_7$ and give a $P$ value for this nucleotide between 155° and 170° (the C2′-endo conformation has $P = 162°$). Only two different coupling values are available for $C_8$, resulting in a less well defined value of $P$ than that for $U_7$. These are consistent with $P$ values between 148° and 170° for nucleotide $C_8$. No values of $P$ are consistent with the data for $U_9$. This situation arises when sugars are not conformationally pure. The value of $J_{1'-2'}$ for $U_9$ shows that a significant (10%) population of the sugars are N-type.

The value of $J_{1'-2'}$ poorly defines the specific value of $P$ for N-type sugars. $P$ values between 305° and 50° are consistent with $J_{1'-2'}$ being less than 2 Hz. The inclusion of $\sum J_{2'}$ and $\sum J_{3'}$ data allows $P$ to be defined quite well. For $U_6$, the coupling data are consistent with $P$ values between 0° and 20°. For $U_5$, $A_{11}$, and $C_{12}$ only one extra coupling constant is available, so these values are less well determined. Still, all values are consistent with a C3′-endo conformation ($P = 18°$). The coupling data for $G_{10}$ are not consistent with any value of $P$, again due to the equilibrium between N- and S-type sugar conformations (70/30 N/S). The values of $P$ calculated for the sugars are summarized in column 2 of Table III.

### *Structure of Hairpin*

*Nucleotide Conformation.* Analysis of the coupling constant data yields reasonable estimates of the ribose conformations. Once the ribose conformation has been determined, NOE data can be used to determine the value of the glycosidic torsion angle ($\chi$). Table IV lists the intranucleotide distances determined by the NOE data. Approximate values of $\chi$ were determined from the H8/H6–H3′ or H2′ distance as described under Materials and Methods. All nucleotides have an anti value of $\chi$. Where only the H8/H6–H1′ NOE is available, an approximate value of $\chi$ was not determined, since the H8/H6–H1′ distance does not depend steeply on $\chi$ in the anti range. For the stem residues that could be analyzed, the values of $\chi$ ranged between −170° and −180°. The values observed from crystal structures of A-form RNA are between −160° and −175° (Saenger, 1984). Thus, the stem nucleotides adopt standard A-form conformations.

Table IV: Intranucleotide Proton–Proton Distances (Å) in the RNA Hairpin Calculated from 80-ms NOESY[a]

| nucleotide | H8/H6–H1′ | H8/H6–H2′ | H8/H6–H3′ | H1′–H2′ |
|---|---|---|---|---|
| $G_1$ | | | | |
| $C_2$ | <4 | | 2.8 | <3 |
| $G_3$ | 3.8 | | | 2.6 |
| $A_4$ | 3.5 | | 3.1 | 2.7 |
| $U_5$ | <4 | | | 2.5 |
| $U_6$ | 3.7 | | 2.8 | 2.7 |
| $U_7$ | 3.5 | (2.4) | | 2.9 |
| $C_8$ | 3.5 | (2.4) | | <3 |
| $U_9$ | <4 | (2.4) | | 2.9 |
| $G_{10}$ | <4 | (3.1) | | 2.5 |
| $A_{11}$ | <4 | | 3.3 | 2.7 |
| $C_{12}$ | 3.5 | | 2.8 | 2.6 |
| $C_{13}$ | 3.8 | | | 2.6 |
| $G_{14}$ | 3.8 | | 3.2 | 2.7 |
| $C_{15}$ | 3.7 | | 2.8 | 2.6 |
| $C_{16}$ | 3.8 | (3.7) | (2.6) | <3 |

[a] Distances in parentheses are for nucleotides with significant populations of both N and S conformers; this results in $1/r^6$ averaging of the distance determined by NOE and inaccurate distances; distances marked with (<) are particularly imprecise, usually due to spectral overlap. Estimated error in distances is ±0.3 Å.

The loop residues adopt the C2′-endo conformation. For anti values of $\chi$, the expected H6–H2′ distance is about 2.0–2.1 Å. The observed distance for all three loop residues was about 2.4 Å, which gave $\chi$ values of about −115 ± 15°. The value of $\chi$ observed for C2′-endo sugars in $tRNA^{Phe}$ is about −100° (Holbrook et al., 1978). The difference between the value of $\chi$ calculated from the NOE data and the value observed in tRNA, although within experimental error, is probably caused by overestimation of this distance due to spin diffusion, resulting from the long (80 ms) mixing time.

*Strand Conformation.* NMR allows fairly precise determination of individual nucleotide conformations. The overall structure of an RNA molecule is defined by the relative orientation of these nucleotides. The internucleotide NOEs allow some elucidation of overall conformation. Particular care must be taken in the interpretation of internucleotide NOEs. Often these distances are quite short; in standard A-form duplexes, the distance from the H8 proton to the 5′-neighboring H2′ proton is expected to be about 2.0 Å. At the mixing times of 80–120 ms, considerable spin diffusion will occur through the H2′ proton. These distances can only be interpreted in terms of an upper limit to the distance. Despite this, the data still allow a semiquantitative analysis of the structure of the hairpin, especially regarding two major features: (1) the structure of the double-helical regions, especially around the region of the A·C apposition, and (2) the structure of the loop region of the hairpin.

*Stem Conformation.* The values for some specific internucleotide distances are listed in Table V. The imino proton data suggest that $G_1$–$U_6$ form a double-helical stem region by pairing with $C_{15}$–$G_{10}$. The H8/H6–H1′ connectivity pathways confirm these results. The majority of nucleotides in this stem region adopt N-type sugar conformations, with values of $\chi$ consistent with the formation of an A-form stem. The internucleotide $^{3'}H8/H6–^{5'}H_2'$ distances for nucleotides $C_{16}$–$A_{11}$ are all quite short (<2.4 Å). This is also consistent with the formation of an A-form duplex by these residues. A few $^{3'}H8/H6–^{5'}H3'$ distances could be measured; for example, the $G_{14}(H8)$–$C_{13}(H3')$ distance is 3.0 Å. In crystal structures

Table V: Estimated Internucleotide Proton–Proton Distances (Å) in the RNA Hairpin[a]

| proton | H6/H8–5′(H2′) | H6/H5/H8–5′(H3′) |
|---|---|---|
| $C_{16}(H_6)$ | <2.4 | OL |
| $C_{15}$(H6) | <2.4 | OL |
| $G_{14}$(H8) | <2.4 | 3.0 |
| $C_{13}$(H6) | <2.4 | OL |
| $C_{12}$(H6) | <2.4 | OL |
| $A_{11}$(H8) | (2.4) | (2.8) |
| $G_{10}$(H8) | | 3.3 |
| $U_9$(H6) | | |
| $C_8$(H6) | ~4 | 2.6 |
| $C_8$(H5) | | 3.1 |
| $U_7$(H6) | | |
| $U_6$(H6) | <2.4 | |
| $U_5$(H6) | 2.6 | OL |
| $A_4$(H8) | <2.4 | |
| $G_3$(H8) | <2.4 | 3.0 |
| $C_2$(H6) | <2.4 | |

[a] Distances were estimated from intensities of NOE cross peaks at an 80-ms $\tau_{mix}$. The (<) symbolizes that the distance is an upper limit due to spin diffusion; OL means that the cross peak could not be integrated due to spectral overlap. Distances in parentheses may be unreliable, since the sugar conformations are not pure (see Table II). Estimated precision is ±0.5 Å.

of A-form helices, this distance is about 3.0–3.1 Å. Nucleotide $C_{16}$ stacks in an A-like fashion at the 3′ terminus of the stem, as inferred from the strong $C_{16}$(H6)–$C_{15}$(H2′) NOE. The $C_{16}$ ribose appears to have more conformational freedom than the ribose sugars from base-paired nucleotides.

The A-form geometry includes $C_{12}$, which is part of the $A_4$·$C_{12}$ apposition. $C_{12}$ adopts a pure C3′-endo sugar conformation ($P = -20°$ to $+20°$), with an anti value of $\chi$. The $A_{11}$(H2) proton gives an NOE to the $C_{12}$(H1′) proton as well as a cross-strand NOE to the $U_6$(H1′) proton. These NOEs show that $A_{11}$ is positioned in an A-form geometry with respect to these nucleotides. The internucleotide $^3$H6–$^5$H2′ distances for $C_{13}$–$C_{12}$–$A_{11}$ are all short, as expected for an A-form helix. The only significant evidence of distortion due to the A·C apposition is that the ribose sugar of $C_{13}$ exhibits some conformational flexibility (25% S-type sugar).

The 5′ side of the hairpin stem exhibits similar characteristics of an A-form geometry. All the nucleotides have pure N-type sugars with anti glycosidic torsion angles. The H8/H6–H2′ distances from $A_4$ to $G_3$ and from $G_3$ to $C_2$ are short (<2.4 Å), consistent with an A-like geometry. The $G_3$-(H8)–$C_2$(H3′) distance is 3.0 Å, again in agreement with an A-form geometry. The NOEs from $C_2$ to $G_1$ are weak, but this is most likely a result of end-fraying effects. Weak NOEs characteristic of end fraying are not observed at the 3′ side of the helix, possibly due to the presence of the dangling $C_{16}$.

The $U_6$(H6)–$U_5$(H2′) distance is short, but there appears to be some distortion in the step from $U_5$ to $A_4$, as the H6–H2′ distance is slightly longer (2.6 Å) than standard A-form geometry. Since the same long distance is determined from either 80- or 120-ms NOESY data, the problem does not seem to be spin diffusion. Despite this minor distortion, $A_4$ is incorporated into the helix in a fairly regular A-like geometry. The best evidence is the NOEs from $A_4$(H2): the $A_4$(H2) proton gives NOEs to the $U_5$(H1′) proton and cross strand to the $C_{13}$(H1′) proton. These NOEs are expected for A-form geometry since the A(H2) proton is near the center of the base pair, as opposed to the other aromatic and sugar protons, which are situated on the perimeter. The presence of the cross-strand NOE from $A_4$(H2) to $C_{13}$(H1′) requires that the $A_4$(H2) proton be in close proximity to the cross strand. This condition can only be satisfied if $A_4$ is incorporated into the helix and if the nature of the distortion from $U_5$ to $A_4$ is subtle. Since

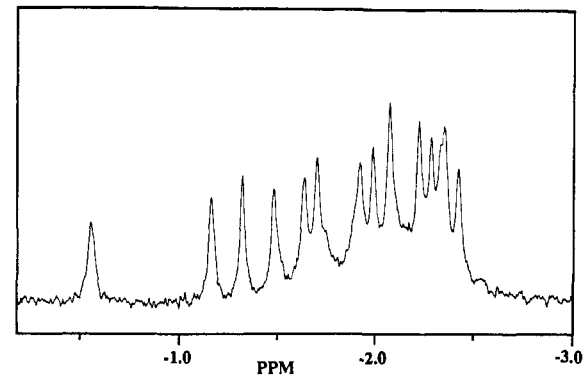


FIGURE 7: $^1$H-broad-band-decoupled $^{31}$P NMR spectrum in 50 mM NaCl, 10 mM sodium phosphate, pH 6.3, and 0.1 mM EDTA at 25 °C. The spectrum is referenced to $H_2PO_4^-$.

both $A_4$ and $C_{12}$ are incorporated into the helix, they are most likely hydrogen bonded. The potential hydrogen-bonded structures and the evidence for their existence will be discussed below.

*Loop Conformation.* The loop region consists of three nucleotides ($U_7$, $C_8$, $U_9$) that cross the A-form stem over the $U_6$·$G_{10}$ base pair. On the 3′ side of the loop, the stem nucleotide $G_{10}$ has NOE connectivities to the first loop nucleotide, $U_9$. The ribose sugar of $U_9$ is stacked in proximity to the base of $G_{10}$; the $G_{10}$(H8)–$U_9$(H3′) distance is 3.3 Å. There is not a short $G_{10}$(H8)–$U_9$(H2′) distance, as expected in a helical region. Instead, the $G_{10}$(H8) proton is relatively close to the $U_9$(H4′) proton (distance ≈ 3 Å). The ribose sugars for both $G_{10}$ and $U_9$ exhibit some conformational lability: $G_{10}$ is 30% S-type, whereas $U_9$ is 10% N-type. There are no NOE connectivities between $U_9$ and $C_8$. The short distances between $C_8$ and $U_7$ are indicative of the unique loop conformation. The $C_8$(H6) proton is quite close to the $U_7$(H3′) proton (2.6 Å) and far from the $U_7$(H2′) proton (ca. 4.0 Å). The $C_8$-(H5)–$U_7$(H3′) distance is short (3.0 Å). There is also a short distance (<3.5 Å) from the $C_8$(H5) proton to the tentatively assigned $U_7$(H5′/5″) proton. These NOEs show that the base portion of $C_8$ is stacked upon the sugar of $U_7$. The NOE connectivity between the final loop residue ($U_7$) and the first nucleotide on the 5′ side of the stem ($U_6$) is tenuous. A single very weak NOE cross peak is observed in the 400-ms NOESY spectrum between the $U_7$(H6) and the $U_6$(H2′) protons. The stem nucleotides on the 5′ side of the loop show very little flexibility in their ribose conformations.

*$^{31}$P Spectrum.* Further evidence for a unique loop conformation comes from the WALTZ-decoupled $^{31}$P spectrum at 25 °C (Figure 7). The spectrum has a large chemical shift dispersion (>2 ppm) and is very well resolved. A total of 15 resonances are observed within this region, which accounts for the 15 internal phosphate groups. The upfield peaks in the $^{31}$P spectrum (−1.8 to −2.5 ppm) are correlated to phosphate groups with $g^-$,$g^-$ phosphodiester torsion angles, ($\alpha$, $\zeta$) (Gorenstein, 1981; Gorenstein et al., 1988). The nine resonances that fall in this shift range most likely arise from phosphate groups within A-form helical regions. The intriguing resonances are the six downfield peaks between −0.6 and −1.9 ppm. Generally, if either phosphate torsion angle ($\alpha$ and $\zeta$) adopts a trans-like value, the $^{31}$P resonances are shifted downfield. The resonance far downfield at −0.6 ppm is in a chemical shift region characteristic of Z-form helices, which have $g$–$t$ torsion angles for CpG dinucleotide steps (Eckstein, 1985; Saenger, 1984; Davis et al., 1986). This resonance is almost definitely due to a trans value of either $\alpha$ or $\zeta$. The other downfield resonances are also consistent with non-A-form torsion angles.

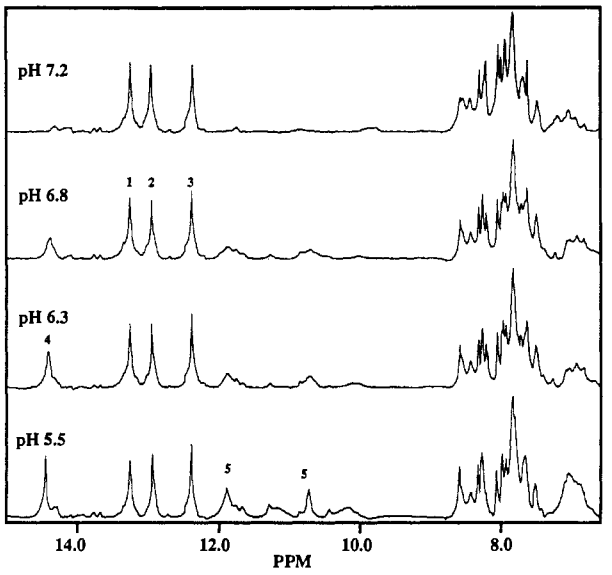


FIGURE 8: pH dependence of the exchangeable proton NMR spectrum in 50 mM NaCl, 10 mM sodium phosphate, and 0.1 mM EDTA at 15 °C. Peaks are numbered as in Figure 2c.

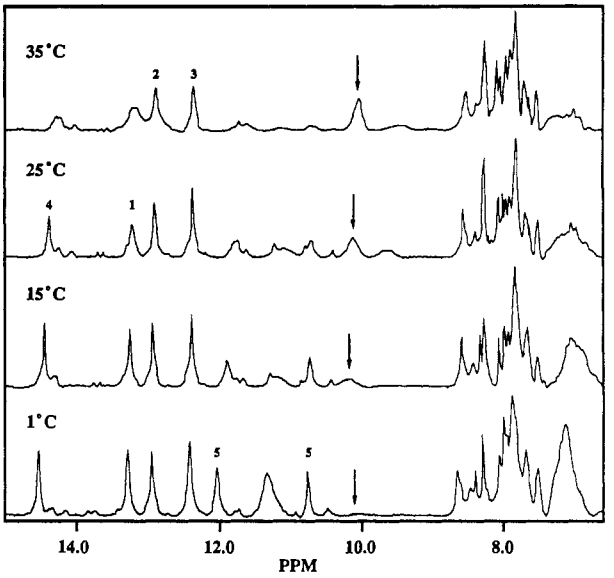


FIGURE 9: Temperature dependence of the exchangeable proton NMR spectrum at pH 5.5 in 50 mM NaCl, 10 mM sodium phosphate, and 0.1 mM EDTA. The arrow indicates the amino resonance(s) that sharpen(s) with increasing temperature as the imino proton resonances broaden.

These may be due to true static variation from $g^-,g^-$ torsion angles or to phosphate groups with conformational freedom (i.e., some population of trans torsion angles).

The $^{31}P$ resonances were not assigned to specific phosphate positions. The downfield resonances may be due to phosphates near the A·C or G·U appositions or to phosphates within the loop region. Gorenstein et al. (1988) have assigned the $^{31}P$ resonances within a DNA dodecamer containing a G·T mispair. The farthest downfield $^{31}P$ resonance was assigned to the phosphate group 3′ to the G·T mismatch site. This resonance was shifted downfield from the center of the envelope of B-form peaks by only 0.5 ppm. Since $A_4$ and $C_{12}$ are incorporated into the A-form duplex, it is unlikely that a major distortion, necessary to cause a large downfield shift, is occurring. It is probable that the backbone distortion is occurring within the loop region or at the junction between the loop and stem regions. Such changes in backbone angles are observed in the loops of $tRNA^{Phe}$ and result in $\pi$-turns (Saenger, 1984). These turns allow sharp changes in direction of the phosphodiester backbone, which may be required in the hairpin loop to bridge the A-form stem (a distance of about 11 Å). Zhang et al. (1989) observed downfield $^{31}P$ resonances for fragments of 5S rRNA with three nucleotide hairpin loops. A downfield shift of 1 ppm of the $^{m5}C_3pG_4$ $^{31}P$ resonance in the two-base DNA hairpin loop $^{m5}CG^{m5}CGTG^{m5}CG$ was observed by Orbons et al. (1987a,b).

*Effect of pH.* Figure 8 illustrates the effects of pH on the NMR spectrum of the exchangeable protons at 15 °C. At pH 5.5, the imino resonances are relatively sharp. The broad peak centered at 10.0 ppm will be discussed below. As the pH is raised, the line widths of the two G·U imino resonances, the A·U resonance, and the loop imino resonances all increase. The line widths of the three G·C resonances comprising the stem of the hairpin all remain relatively constant up to pH 7.8. At pH 7.2, only these three resonances are observed. The line width of each resonance depends on the contributions of dipolar coupling and exchange. If the effect of exchange is negligible, then the spectrum should sharpen as the temperature is raised; the opposite is expected if the exchange contribution is significant. If the exchange is limited by the opening of the base pairs (open limited), then the exchange rate should be independent of buffer concentration; however, if the exchange is not open limited, then the line width (exchange rate) will be affected by buffer concentration (Teitelbaum & Englander, 1975; Guéron et al., 1987; Leroy et al., 1988; Benight et al., 1988).

The imino resonances of the hairpin are grouped into two categories. The three resonances from the G·C pairs are unaffected by the change in pH. These resonances are relatively well protected from solvent exchange. In contrast, the $U_5$·$A_{11}$ and $U_6$·$G_{10}$ imino resonances are broadened at higher pH. Increasing the pH also increases the concentration of base catalyst. Thus either the exchange of these protons is limited by base catalysis or the structure formed is dependent on pH, such that at higher pH the loop conformation is destabilized. The broad peak at 10.0 ppm at pH 5.5 is most likely due to amino protons. Figure 9 shows that as the temperature is raised, the imino resonances broaden whereas the resonance at 10.0 ppm sharpens; a second broad peak at about 9.6 ppm is observed above 25 °C. Amino resonances from adenine and guanine are broad due to rotational exchange about the C–N bond (McConnell & Seawell, 1972; McConnell, 1984). The rotational exchange rate increases at higher temperature and thus the lines sharpen, resulting in a single resonance for the two amino protons. The peaks at ca. 9 ppm are also probably adenine amino resonances, since they also sharpen with temperature. Protonation within the $A_4$·$C_{12}$ base pairs would create a charged environment, affecting primarily the $A_4$ amino proton but also the $A_{11}$ amino proton in the adjacent base pair. On the basis of these criteria, the resonance at 10.0 ppm is the $A_4$(amino) proton, and the upfield peak (ca. 9 ppm) is the $A_{11}$(amino) proton. At pH 6.3, no NOEs were observed from either of these amino peaks. At higher pH (7.2), the amino resonance at 10 ppm has broadened into base line and only a broad resonance (Figure 8) is observed upfield (at 9.4 ppm). Similar behavior has been observed in studies of oligodeoxynucleotides containing an A·C mispair (Kalnik et al., 1988a).

The nonexchangeable NMR spectrum is also sensitive to pH (Figure 10). The resonances are all relatively sharp at pH 5.5, but certain resonances broaden as the pH is raised. The resonance that broadens at lowest pH is the $A_4$(H2) resonance at 8.29 ppm. This resonance is broadened even at pH 6.3, and the center of the broad peak shifts upfield at pH

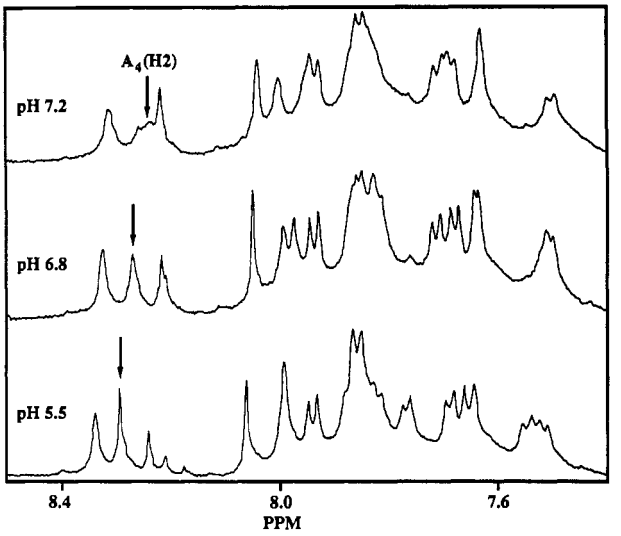


FIGURE 10: pH dependence of the nonexchangeable proton NMR spectrum in 50 mM NaCl, 10 mM sodium phosphate, and 0.1 mM EDTA at 15 °C. The H8/H6/H2 region of the spectrum is shown; the arrow indicates the $A_4$(H2) resonance that broadens and shifts upfield with increasing pH.

7.2. Other peaks also broaden and shift as the pH is raised above 6.8. The $A_4$(H8) and $A_{11}$(H8) peaks overlap at pH 5.5; as the pH is raised, the $A_4$(H8) signal shifts upfield and eventually broadens. At pH 7.2, the $A_4$(H8) resonance is a broad shoulder on the $U_7$(H6) peak at 7.95 ppm. The $U_5$(H6) and $C_{15}$(H6) resonances overlap at about 7.55 ppm at pH 5.5. As the pH is raised, one of these resonances broadens, such that only one H6 resonance remains at pH 7.2. The $G_{10}$(H8) resonance downfield at 8.32 ppm also broadens as the pH is raised.

NOESY and DQF-COSY spectra at pH 7.2 were acquired at 25 °C (data not shown). The COSY spectrum contains only eight H5–H6 cross peaks instead of the expected ten. Comparison of the NOESY spectrum at pH 7.2 to that at pH 6.3 revealed that $U_5$(H6) and $C_{12}$(H6) are the two pyrimidines whose signals broaden. The $A_4$(H8) resonance is present, but the $A_4$(H1′) and $A_4$(H2) peaks have broadened at pH 7.2. The H1′–H2′ region of the DQF-COSY contains strong cross peaks from the three loop residues. Most of the loop resonances have similar chemical shifts at pH 6.3 and 7.2.

The pH data are consistent with the formation of a protonated A·C base pair between $A_4$ protonated at the N1 position and $C_{12}$. A·C base-pair formation and incorporation into B-DNA helices have been observed by crystallography and NMR (Hunter et al., 1986; Kalnik et al., 1988a). The proposed A·C mispair structure is shown in Figure 11. The adenine is assumed to be in its major tautomeric form. Protonation changes the local electrostatic environment; protons near the site of protonation [$A_4$(N1)] will have different chemical shifts in the protonated and unprotonated forms. Since the exchange between protonated and unprotonated forms results in broadening, the process must occur on the millisecond time scale. As the pH is raised, the broad $A_4$(H2) resonance shifts upfield, consistent with a fast-exchange process.

The resonances from nucleotides in the stem near the A·C mispair are most affected by changes in pH. The $A_4$(H2) proton is closest to the proposed site of protonation [$A_4$(N1)]; this resonance is broadened at pH 6.3. Some affected resonances, such as the $A_4$(H8), $A_4$(H1′), and $C_{12}$(H6) peaks, are from protons on the nucleotides directly involved in the protonated base pair. Other resonances [$U_5$(H6), $G_{10}$(H8)]

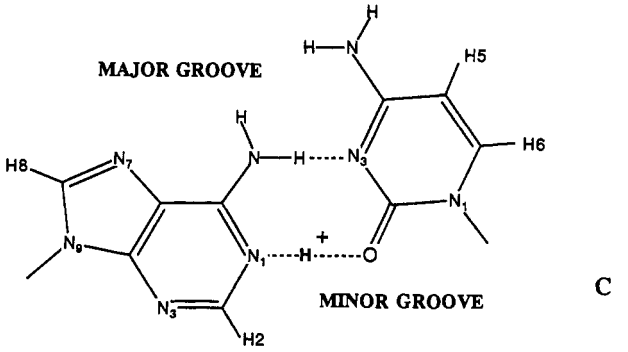


FIGURE 11: Proposed model for the formation of a protonated $A^+$·C base pair, based on the crystallographic results of Hunter et al. (1986).

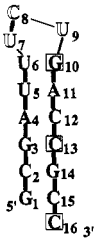

FIGURE 12: Summary of the NMR structural data for the hairpin loop. The sugar conformation is coded by letter type. The C3′-endo conformation is indicated by boldface type and the C2′-endo by outline; an equilibrium between sugar conformations is indicated by a box. Nucleotides all adopt anti glycosidic torsion angles. Internucleotide NOEs are indicated by lines connecting nucleotides. Thick lines indicate strong internucleotide ($^3$H6/H8–$^3$H2′) NOEs consistent with formation of an A-form helix. The internucleotide NOEs are weak between $U_6$ and $U_7$ and between $U_9$ and $G_{10}$. No NOEs are observed between $C_8$ and $U_9$. There is a strong NOE between the $C_8$(H6) and $U_7$(H3′) protons.

correspond to neighboring nucleotides. The base pairs that close the loop, the $U_5$·$A_{11}$ and $U_6$·$G_{10}$ pairs, are more labile at higher pH. In the absence of protonation, the A·C pairing may not be stable. Thus, some of the broadening of resonances at higher pH may be due to structural exchange between, for example, the closed and open loop structures shown in Figure 1.

The $pK_a$ of the N1 position of adenine in free nucleosides is about 4; the $pK_a$ may increase when the protonated site is included within a nucleic acid duplex (Hunter et al., 1986). There is no evidence from our data for minor tautomer formation. Similar protonated forms of adenine are observed in crystal structures of ApA dimers (Saenger, 1984). The negative electrostatic potential of the nucleic acid helix will contribute to a $pK_a$ shift. For example, protonated $C^+$·C base pair formation has been observed in DNA duplexes at near neutral pH.

*Structural Model.* The NMR data can be incorporated into a low-resolution structural model, containing the following important aspects (summarized in Figure 12): (1) The stem forms an A-type helix; the nucleotides in the stem have anti values of $\chi$ and C3′-endo sugar conformations. (2) The 3′-dangling $C_{16}$ stacks at the end of the helix in an A-like fashion. (3) The $A_4^+$·$C_{12}$ mismatch is incorporated into the helix, with perhaps a slight distortion between $U_5$ and $A_4$; protonation of $A_4$ at the N1 position would allow formation of two hydrogen bonds between $A_4$ and $C_{12}$. (4) The $U_6$·$G_{10}$ base pair forms and closes the loop structure. (5) The loop nucleotides all adopt C2′-endo sugar conformations. (6) Certain P–O bonds, most likely in the loop, adopt a trans conformation instead of the usual gauche. (7) $C_8$ stacks upon the sugar of $U_7$. (8)

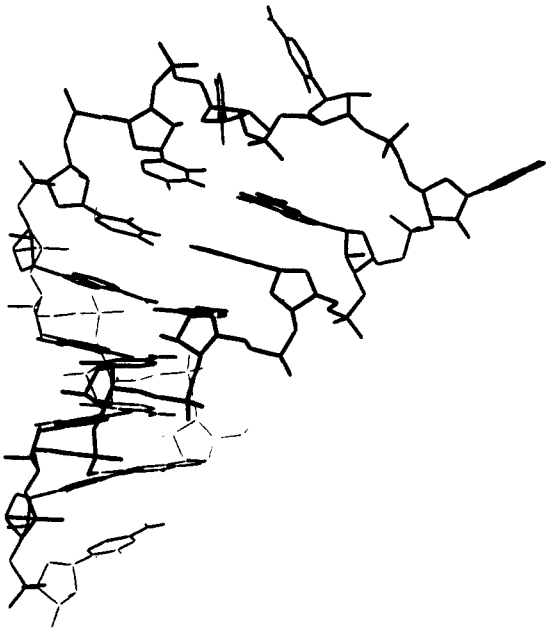

FIGURE 13: Model showing a hairpin with an A-form stem and a loop conformation consistent with the NMR data. The helical stem region is formed by nucleotides $G_1$–$U_6$ and $G_{10}$–$C_{15}$. The 5′-terminal G is in the background on the lower right. The $A^+$·C mispair is incorporated into the helix with little distortion. The three-nucleotide loop runs 5′ to 3′ left to right. $C_8$ is stacked on the sugar of $U_7$; $U_9$ is far from $C_8$, as there is no NOE connectivity between the two nucleotides. The sugar conformations of the three loop nucleotides are C2′-endo.

The ribose sugar of $U_9$ stacks on the base of $G_{10}$.

The model shown in Figure 13 is consistent with the NMR data. It illustrates the gross structural features of the hairpin. The incorporation of an A·C mispair into a double helix has been observed in both crystal and solution structures of B-form DNA (Hunter et al., 1986; Kalnik et al., 1988a). G·T mispairs also fit into B-DNA duplexes (Brown et al., 1985; Kalnik et al., 1988b). These base pairs have approximately the same C1′–C1′ distance as standard Watson–Crick pairs (10.3 versus 10.9 Å). For both A·C and G·U, the major difference from Watson–Crick base pairs is a shift of the purine toward the minor groove and a shift of the pyrimidine toward the major groove; this allows the proper base-pairing geometry. Figure 13 shows the A-form stem; the A·C mispair is easily incorporated into the helix.

The width of a base pair is about 11 Å (C1′–C1′). By adopting a C2′-endo conformation, the intrastrand phosphate–phosphate distance is increased to ca. 7.0 Å from 5.8 Å, if other torsion angles remain constant. Thus, the three nucleotides of the hairpin loop can easily bridge the distance across the base pair, as shown in Figure 13. By adopting C2′-endo puckers, the loop nucleotides are free to engage in structural interactions (and stabilize the hairpin). Such interactions would be restricted if the nucleotides remained C3′-endo, due to the shorter distance spanned. Additional stretching of a nucleotide can be achieved by changing the value of $\gamma$ from the normal gauche$^+$ to trans conformation. However, it is difficult to assign H4′ and H5′/5″ resonances, so that these angles cannot be determined in the loop region. $C_8$ and $U_7$ interact through stacking interactions, as does the $U_9$ ribose with $G_{10}$. It is apparent that certain P–O bonds in the loop adopt unique trans-type conformations.

### *Thermodynamic Stability*

The thermodynamic parameters for the melting of the hairpin in 50 mM NaCl and 10 mM sodium phosphate, pH 6.3, were obtained from analysis of UV absorbance melting curves and are listed in Table VI. The melting temperature changes relatively little upon addition of $Mg^{2+}$; the $T_m$ shifts only 7 °C, to 59 °C, upon addition of 5 mM $Mg^{2+}$. This is reflected in only a slight change in the $\Delta G°$(37 °C) of formation in the presence versus the absence of $Mg^{2+}$ (0.5 kcal/mol more favorable). The stability of the hairpin is reflected in the large $\Delta H°$ of formation (−37.5 kcal/mol in the absence of $Mg^{2+}$). The enthalpic contribution of the three G·C pairs in the stem is calculated to be only −22 kcal/mol (Freier et al., 1986). The loop thus gains an enthalpic stabilization of about −15 kcal/mol by formation of the extra base pairs. The thermodynamic behavior of a hairpin with an A·U base pair instead of the A·C mismatch was measured (Table VI). The $T_m$ of this A·U hairpin in 50 mM NaCl and 10 mM sodium phosphate, pH 6.4, is 64 °C, which is 12 °C higher than that of the A·C hairpin. The A·U hairpin gains considerable enthalpic stabilization ($\Delta\Delta H°$ = −12.4 kcal/mol) over the A·C hairpin. The A·C mismatch in this hairpin results in a free energy of destabilization of the structure relative to an A·U base pair [$\Delta\Delta G°$(37 °C)] of +2.1 kcal/mol. Similar destabilization of A·C mispairs have been observed in DNA (Aboul-ela et al., 1985).

Table VI: Thermodynamic Parameters for Hairpin Formation[a]

| sequence | $T_m$ (°C) | $\Delta H°$ (kcal/mol) | $\Delta S°$ [cal/(mol·K)] | $\Delta G°$(37 °C) (kcal/mol) |
|---|---|---|---|---|
| (A·C)[b,c] | 52.5 | −37.5 | −115 | −1.9 |
| (A·U)[b,d] | 64 | −50 | −148 | −4.0 |
| (A·C)[c,e] | 59.5 | −36 | −108 | −2.4 |

[a] Estimated precision: $T_m$, ± 1 °C; $\Delta H°$, ±5 kcal/mol; $\Delta S°$, ±10 cal/(mol·K); $\Delta G°$, ±0.2 kcal/mol. [b] In 50 mM NaCl, 10 mM sodium phosphate, pH 6.4, and 0.1 mM EDTA. [c] The sequence is that shown in Figure 1. [d] The sequence is the same as shown in Figure 1 except that $C_{12}$ has been changed to $U_{12}$. This replaces the A·C apposition by an A·U pair. [e] In 5 mM $MgCl_2$, 50 mM NaCl, and 10 mM sodium phosphate, pH 6.4.

Hairpin loops of three nucleotides are about 1 kcal/mol less stable than loops of four (Groebe & Uhlenbeck, 1988); loop sizes of nine nucleotides were found to be less stable than the smaller loop sizes by 1–2 kcal/mol. The destabilization due to the A·C mispair must be less than 1.5–2.5 kcal/mol for the three-nucleotide hairpin loop to form. This estimated upper limit to the destabilization due to an A·C mispair is consistent with the destabilization of about +2 kcal/mol for the A·C mispair relative to a Watson–Crick A·U base pair. Lower pH stabilizes the structure. The melting behavior at pH 5.5 and 6.3 is similar; the $T_m$ drops 5 °C at pH 7.2. This corresponds to a free energy of destabilization [$\Delta\Delta G°$(37 °C)] of about 1 kcal/mol at pH 7.2. In contrast, the melting temperature of the A·U hairpin does not depend on pH. The positive free energy of destabilization of the A·C mismatch is compensated by the negative free energy of forming the extra base pairs and the smaller loop.

## CONCLUSIONS

The results presented here illustrate the structural versatility of a relatively simple RNA molecule. The 16-nucleotide sequence forms a hairpin structure with three nucleotides in the loop region and a double-stranded A-form stem incorporating both $A^+$·C and G·U mispairs. The $A^+$·C pair involves protonation of the adenine, most likely at the N1 position. The formation of the three extra base pairs results in a smaller loop (three nucleotides) compared to the open, non-base-paired structure (nine nucleotides). The stabilization of forming the extra loop base pairs offsets the destabilization due to $A^+$·C pair formation.

Both A·C and G·U appositions are common in proposed RNA secondary structures (Noller, 1984), and G·U pairing has been observed in crystal structures of tRNAs (Holbrook et al., 1978). The geometry of the A·C and G·U pairs is slightly different from that of Watson–Crick pairs; these base pairs subtly affect the overall geometry of the A-form duplex. The three extra base pairs in the model of the hairpin (Figure 13) appear less twisted and more ladderlike than the three G·C pairs. Such changes in helical geometry may serve as recognition sites for protein binding. McClain et al. have proposed that a specific distortion caused by a G·U pair in the acceptor stem of *amber* suppressors of $tRNA^{Ala}$ is crucial to the recognition by cognate synthetase; similar enzymatic activity was observed when the G·U pair was replaced by other mispairs but not by Watson–Crick pairs (McClain et al., 1988a). Genetic analysis suggests that A·C pairings can substitute for Watson–Crick pairings in helical regions in phage T4 $tRNA^{Ser}$ (McClain et al., 1988b). Non-Watson–Crick purine–pyrimidine pairings have been proposed in loop regions of 5S rRNA by both NMR and chemical modification studies (Gewirth, 1988; Romaniuk et al., 1988; Romby et al., 1988; Westhof et al., 1989).

The stability of the G·U pairing is approximately equivalent to that of an A·U pair (Sugimoto et al., 1986). For this reason, G·U appositions in RNA secondary structures are usually considered as base paired and incorporated into helical regions. A·C appositions are more unstable, yet the results presented here indicate that A·C can form a hydrogen-bonded base pair that can be incorporated into a relatively short helical region.

The loop folding model of Haasnoot and Hilbers emphasized the A-form stacking possible on the 3′ side of loops, such that loops of seven to eight nucleotides would be most stable (Haasnoot et al., 1986). However, formation of either Watson–Crick or non-Watson–Crick base pairs should allow similar stabilization. The results described here demonstrate that small loops can form stable structures in RNA. It is likely, in analogy to DNA, that even two-nucleotide loops will be possible (Orbons et al., 1987a,b; Blommers et al., 1989). In the hairpin we have studied, the loop nucleotides all have a C2′-endo conformation; none of the nucleotides in the anticodon loop of $tRNA^{Phe}$ adopt a C2′-endo pucker. Whether a ribonucleotide adopts a C2′-endo pucker seems to depend on its structural context. The C2′-endo and C3′-endo puckers have similar energies in free nucleotides. Within an A-form duplex, the C3′-endo pucker may be stabilized by hydrogen bonding between the O2′ hydrogen and the O4′ in the 3′-neighboring sugar (Saenger, 1984). Such structural constraints may occur in well-stacked, larger loops (like tRNA) but not in smaller loops. Although the loop nucleotides $C_8$ and $U_9$ are stacked, the stacking is not in the A-form geometry constrained by helical structure.

Loop structure and stability can also be affected by the nature of the base pair that borders the loop (the closing base pair). The studies of the common four-nucleotide loop sequence (-UUCG-) found in many RNAs showed that switching the closing base pair from C·G to G·C lowered the $T_m$ by 5 °C (Tuerk et al., 1988). This may reflect specific interactions favored by a particular base-pair orientation. The results presented here show that G·U pairs can serve as the closing base pair for a three-base loop. In the *E. coli* 16S rRNA secondary structure, potential G·U pairs are often found at or near the junctions between stem and loop regions (Noller, 1984; Stern et al., 1988). It is intriguing to note that the hairpin termination signal in the *trp* leader region can be drawn as a three-base hairpin loop closed by a U·G pair followed by an A·C mismatch; the structure of this hairpin is generally drawn as a four-base loop with a bulged A (Yanofsky, 1981).

The small size of most RNA helical regions and the relative inaccessibility of the major groove of RNA make it unlikely that RNA-binding proteins will recognize a sequence within a duplex region, as do certain site-specific DNA-binding proteins (Pabo & Sauer, 1984). Instead, RNA-binding proteins will more likely recognize the overall three-dimensional conformation of the RNA, specific structural features of a particular domain, or a sequence within a non-base-paired region (Stern et al., 1989; Rould et al., 1989). The recognition of cognate tRNAs by specific aminoacyl-tRNA synthetases requires specific nucleotides that distinguish various tRNAs (Hou & Schimmel, 1988; McClain & Foss, 1988; McClain et al., 1988a; Sampson et al., 1989) in addition to the three-dimensional folding probably common to all tRNAs (Romby et al., 1985). Recognition of relatively simple structures has also been shown to be specific for conformation rather than sequence. The coat proteins from bacteriophages R17 and Qβ bind specifically to RNA hairpins; the structure of the hairpins is apparently the critical factor in determining specificity (Wu & Uhlenbeck, 1987; Witherell & Uhlenbeck, 1989). The structure of the stem–loop studied in this paper reveals some of the specific local features of conformation that may be important for recognition of RNA. These include non-Watson–Crick base pairs ($A^+$·C and G·U), which change helix geometry, and specific loop conformations.

## Acknowledgments

We thank David Koh for synthesizing DNA oligonucleotides, Barbara Dengler for general assistance, and Jeff Pelton and John Hubbard for their assistance with the computer graphics facility. We also thank Prof. David Wemmer, Dr. Peter Davis, and Dr. Gabriele Varani for advice and useful discussions.

## References

Aboul-ela, F., Koh, D., Tinoco, I., Jr., & Martin, F. H. (1985) *Nucleic Acids Res. 13*, 4811–4824.

Altona, C. (1982) *Recl.: J. R. Neth. Chem. Soc. 101*, 413–434.

Bax, A., & Lerner, L. (1988) *J. Magn. Reson. 79*, 429–438.

Benight, A. S., Schurr, J. M., Flynn, P. F., Reid, B. R., & Wemmer, D. E. (1988) *J. Mol. Biol. 200*, 377–399.

Blommers, M. J. J., Walters, J. A. L. I., Haasnoot, C. A. G., Aelen, J. M. A., van der Marel, G. A., van Boom, J. H., & Hilbers, C. W. (1989) *Biochemistry 28*, 7491–7498.

Bodenhausen, G., Kogler, H., & Ernst, R. R. (1984) *J. Magn. Reson. 58*, 370–388.

Braunschweiler, L., Bodenhausen, G., & Ernst, R. R. (1983) *Mol. Phys. 48*, 535–560.

Clore, G. M., Gronenborn, A. M., Piper, E. A., McLaughlin, L. W., Graeser, E., & van Boom, J. H. (1984) *Biochem. J. 221*, 737–751.

Davis, P. W., Hall, K., Cruz, P., Tinoco, I., Jr., & Neilson, T. (1986) *Nucleic Acids Res. 14*, 1279–1291.

Davis, P. W., Adamiak, R. W., & Tinoco, I., Jr. (1990) *Biopolymers 29*, 109–122.

de Leeuw, F. A. A. M., & Altona, C. (1982) *J. Chem. Soc., Perkin Trans. 2*, 375–384.

Dingwall, C., et al. (1989) *Proc. Natl. Acad. Sci. U.S.A. 86*, 6925–6929.

Eckstein, F. (1985) *Annu. Rev. Biochem. 54*, 367–402.

Feng, S., & Holland, E. C. (1988) *Nature 334*, 165–167.

Freier, S. M., Kierzek, R., Jaeger, J. A., Sugimoto, N., Caruthers, M. H., Neilson, T., & Turner, D. H. (1986) *Proc.*

*Natl. Acad. Sci. U.S.A. 83*, 9373–9377.
Gewirth, D. (1988) Ph.D. Thesis, Yale University.
Gorenstein, D. G. (1981) *Annu. Rev. Biophys. Bioeng. 10*, 355–386.
Gorenstein, D. G., Scroeder, S. A., Fu, J. M., Metz, J. T., Roongta, V., & Jones, C. R. (1988) *Biochemistry 27*, 7223–7237.
Gralla, J., & Crothers, D. M. (1973) *J. Mol. Biol. 73*, 497–511.
Groebe, D. R., & Uhlenbeck, O. C. (1988) *Nucleic Acids Res. 16*, 11725–11735.
Guêron, M., Kochoyan, M., & Leroy, J. L. (1987) *Nature 328*, 89–92.
Haasnoot, C. A. G., Hilbers, C. W., van der Marel, G. A., van Boom, J. H., Singh, U. C., Pattabiraman, N., & Kollman, P. A. (1986) *J. Biomol. Struct. Dyn. 3*, 843–857.
Holbrook, S. R., Sussman, J. L., Warrant, R. W., & Kim, S.-H. (1978) *J. Mol. Biol. 123*, 631–660.
Hore, P. J. (1983) *J. Magn. Reson. 55*, 283–300.
Hou, Y.-M., & Schimmel, P. (1988) *Nature 333*, 140–145.
Hunter, W. N., Brown, T., Anand, N. N., & Kennard, O. (1986) *Nature 320*, 552–555.
Kalnik, M. W., Kouchakdjian, M., Li, B. F. L., Swann, P. F., & Patel, D. J. (1988a) *Biochemistry 27*, 100–108.
Kalnik, M. W., Kouchakdjian, M., Li, B. F. L., Swann, P. F., & Patel, D. J. (1988b) *Biochemistry 27*, 108–115.
Kennard, O. (1985) *J. Biomol. Struct. Dyn. 3*, 205–226.
Leroy, J. L., Kochoyan, M., Huynh-Dinh, T., & Guêron, M. (1988) *J. Mol. Biol. 200*, 223–238.
McClain, W. H., & Foss, K. (1988) *Science 240*, 793–796.
McClain, W. H., Chen, Y.-M., Foss, K., & Schneider, J. (1988a) *Science 242*, 1681–1684.
McClain, W. H., Wilson, J. H., & Seidman, J. G. (1988b) *J. Mol. Biol. 203*, 549–553.
McConnell, B. (1984) *J. Biomol. Struct. Dyn. 1*, 1407–1421.
McConnell, B., & Seawell, P. C. (1972) *Biochemistry 11*, 4382–4392.
Müllner, E. W., & Kühn, L. C. (1988) *Cell 53*, 815–825.
Noller, H. F. (1984) *Annu. Rev. Biochem. 53*, 119–162.
Orbons, L. P. M., van der Marel, G. A., van Boom, J. H., & Altona, C. (1987a) *J. Biomol. Struct. Dyn. 4*, 939–963.
Orbons, L. P. M., van Beuzekom, A. A., & Altona, C. (1987b) *J. Biomol. Struct. Dyn. 4*, 965–987.
Pabo, C. O., & Sauer, R. T. (1984) *Annu. Rev. Biochem. 53*, 293–321.
Pardi, A., Hare, D. R., & Wang, C. (1988) *Proc. Natl. Acad. Sci. U.S.A. 85*, 8785–8789.
Piantini, U., Sørensen, O. W., & Ernst, R. R. (1982) *J. Am. Chem. Soc. 104*, 6800–6801.
Puglisi, J. D. (1989) Ph.D. Dissertation, University of California, Berkeley.
Puglisi, J. D., & Tinoco, I., Jr. (1990) in *Methods in Enzymology, RNA Processing* (Dahlberg, J. E., & Abelson, J. N., Eds.) Vol. 180, pp 304–325, Academic Press, New York.
Puglisi, J. D., Wyatt, J. R., & Tinoco, I., Jr. (1990) *J. Mol. Biol.* (in press).
Rich, A., & RajBhandary, U. L. (1976) *Annu. Rev. Biochem. 45*, 805–860.
Rinkel, L. J., & Altona, C. (1987) *J. Biomol. Struct. Dyn. 4*, 621–649.
Romaniuk, P. J., Lowary, P., Wu, H.-N., Stormo, G., & Uhlenbeck, O. C. (1987) *Biochemistry 26*, 1563–1568.
Romby, P., Moras, D., Bergdoll, M., Dumas, P., Vlassov, V. V., Westof, E., Ebel, J. P., & Giegé, R. (1985) *J. Mol. Biol. 184*, 455–471.
Romby, P., Westhof, E., Toukifimpa, R., Mache, R., Ebel, J.-P., Ehresmann, C., & Ehresmann, B. (1988) *Biochemistry 27*, 4721–4730.
Rould, M. A., Perona, J. J., Söll, D., & Steitz, T. A. (1989) *Science 246*, 1135–1142.
Saenger, W. (1984) *Principles of Nucleic Acid Structure*, Springer-Verlag, New York.
Sampson, J. R., Direnzo, A. B., Behlen, L. S., & Uhlenbeck, O. C. (1989) *Science 243*, 1363–1366.
Stern, S., Weiser, B., & Noller, H. F. (1988) *J. Mol. Biol. 204*, 447–481.
Stern, S., Powers, T., Changchien, L.-M., & Noller, H. F. (1989) *Science 244*, 783–789.
Sugimoto, N., Kierzek, R., Freier, S. M., & Turner, D. H. (1986) *Biochemistry 25*, 5755–5759.
Teitelbaum, H., & Englander, S. W. (1975) *J. Mol. Biol. 92*, 55–78.
Tuerk, C., Gauss, P., Thermes, C., Groebe, D. R., Gayle, M., Guild, N., Stormo, G., D'Aubenton-Carafa, Y., Uhlenbeck, O. C., Tinoco, I., Jr., Brody, E. N., & Gold, L. (1988) *Proc. Natl. Acad. Sci. U.S.A. 85*, 1364–1368.
Uhlenbeck, O. C., Borer, P. N., Dengler, B., & Tinoco, I., Jr. (1973) *J. Mol. Biol. 73*, 483–496.
van den Hoogen, F. (1988) Ph.D. Dissertation, University of Leiden.
van Knippenberg, P. H., & Heus, H. A. (1983) *J. Biomol. Struct. Dyn. 1*, 371–381.
Varani, G., Wimberly, B., & Tinoco, I., Jr. (1989) *Biochemistry 28*, 7760–7772.
Westhof, E., Romby, P., Romaniuk, P. J., Ebel, J.-P., Ehresmann, C., & Ehresmann, B. (1989) *J. Mol. Biol. 207*, 417–431.
Widmer, H., & Wüthrich, K. (1987) *J. Magn. Reson. 74*, 316–336.
Witherell, G. W., & Uhlenbeck, O. C. (1989) *Biochemistry 28*, 71–76.
Wu, H. N., & Uhlenbeck, O. C. (1987) *Biochemistry 26*, 8221–8227.
Wüthrich, K. (1986) *NMR of Proteins and Nucleic Acids*, John Wiley and Sons, New York.
Wyatt, J. R., Puglisi, J. D., & Tinoco, I., Jr. (1990) *J. Mol. Biol.* (in press).
Yanofsky, C. (1981) *Nature 289*, 751–758.
Zhang, P., Rycyna, R., & Moore, P. B. (1989) *Nucleic Acids Res. 17*, 7295–7302.